Soft Matter

PAPER

View Article Online
View Journal

Cite this: DOI: 10.1039/d6sm00114a

Confined labyrinthine pattern in chiral liquid crystal droplets

M. Rubio-Saldías, *[a] V. Fernandez-Gonzalez, [a] M. G. Clerc,[a] P. I. Hidalgo [b] and J. Vergara[b]

Received 6th February 2026,
Accepted 5th May 2026

DOI: 10.1039/d6sm00114a

rsc.li/soft-matter-journal

Systems that continuously inject and dissipate energy tend to self-organize, resulting in complex spatial patterns. Labyrinthine patterns are characterized by an arrangement that exhibits local order while lacking global order. We experimentally investigate the formation of confined textures in temperature-driven chiral liquid crystal droplets. The observed textures are mainly dominated by labyrinthine patterns. To describe the observed textures, we have theoretically examined the system near the winding/unwinding transition. In this region, we can use a simplified description based on an amplitude equation with inhomogeneous coefficients that account for the confinement imposed by the droplet geometry. Numerical simulations of this model show qualitative agreement with the experimental observations. Our findings offer a novel perspective on the confined textures under various geometric configurations.

Nature exhibits a vast diversity of self-organized patterns, from sand dunes and animal fur to fish scales, snowflakes, and cloud formations, that arise in systems driven far from equilibrium.[1–7] These patterns, although diverse, share a common physical origin: the continuous injection and dissipation of energy in macroscopic systems. A general theoretical framework for understanding their emergence relies on the spontaneous breaking of spatial symmetry in otherwise uniform states. Close to this transition, striped, hexagonal, square, and superlattice patterns are observed.[2–8] Superlattices are patterns formed by many modes with the same wavelength.[7,8] A unified approach to describing the emergence and dynamics of these simple patterns is based on the amplitude equations for the critical modes of equilibrium that exhibit a spatial instability.[2,3,7] Patterns are periodic structures that often exhibit defects that break their discrete translational symmetry. As energy injection increases and moves away from spatial instabilities, pattern-forming systems exhibit more complex patterns, characterized by a greater number of defects. An example of these complex patterns is the labyrinthine pattern,[9] which exhibits short-range order described by a single mode and long-range orientational disorder. Namely, these patterns are characterized by a powdered spatial ring spectrum in their Fourier transform and, in turn, exhibit an averaged windowed Fourier transform with a single spatial mode.[9] These disordered patterns have been observed in mussel beds,[10] cardiovascular calcification,[11] phytomass,[12] microemulsions,[13] fish skin,[14] fluid convection,[15] Langmuir monolayers,[16] magnetic fluids,[17] chemical reactions,[18] and chiral liquid crystals,[19] to mention a few. In chiral liquid crystals, labyrinthine textures typically appear in planar cells under thermal or electric driving near the winding/unwinding transition.[19–22]

The characteristic wavelength of these textures is proportional to the pitch, the helical rotation length associated with the molecular chirality. Most previous studies have investigated these phenomena in extended cells with uniform anchoring, where confinement and curvature effects can be neglected. However, when chiral liquid crystals are confined in droplets, geometry imposes boundary constraints that modify the elastic and chiral interactions.[23] Recent experiments have shown that temperature/driven winding/unwinding transitions in chiral liquid crystal droplets can lead to triangular arrays of chiral domains known as Abrikosov clusters.[23]

However, the self-organization and modeling of disordered patterns under confined conditions, such as droplets, remain open problems.

In this work, we experimentally investigate the formation of confined textures in thermally driven chiral liquid crystal droplets. We characterize the discontinuous nature of the winding/unwinding transition and show that confinement and droplet geometry determine the morphology of the resulting labyrinthine patterns. Theoretically describing the observed texture and dynamics using nematic hydrodynamics is a significant challenge. Hence, we focused on the system near the winding/unwinding transition. In this region, we can employ a simplified description based on an amplitude equation with non-homogeneous coefficients that account for the confinement

[a] Departamento de Física and Millennium Institute for Research in Optics, Facultad de Ciencias Físicas y Matemáticas, Universidad de Chile, Casilla 487-3, Santiago, Chile. E-mail: martin.rubio.s@ug.uchile.cl
[b] Departamento de Química Orgánica, Facultad de Ciencias Químicas, Universidad de Concepción, Casilla 160-C, Concepción, Chile

imposed by the droplet geometry. Numerical simulations reproduce the experimental observations qualitatively, providing a consistent framework for understanding confined labyrinthine structures in chiral liquid crystal droplets.

Experimental setup

The experiments were conducted using chiral nematic liquid crystals (CLCs), composed of a nematic liquid crystal E7 (Merck) host doped with the chiral molecule EOS-12 at 10 wt%.[24] CLC droplets were prepared by depositing volumes of CLC using a 0.2–2 l micropipette onto untreated soda-lime glass slides (EDLAB Cat. No. 7105). This procedure does not allow for control of the size and shape of the droplets. Droplets on the substrate anchor homeotropically; for small and large droplets, we observe that on the surface with the air, they anchor approximately homeotropically and orthogonally to the surface. The liquid crystal mixture exhibits a nematic to chiral isotropic transition at 62 °C and from isotropic liquid to chiral nematic crystal at 61.5 °C.[27]

Fig. 1a shows a schematic representation of the experimental setup. The sample with chiral droplets is studied using a polarized optical microscopy (POM; Leica DM2700P) inside a thermal chamber (TC; Mod. LTS350E), which provided a temperature control and adjustable heating and cooling rates, with a precision of ±0.005 °C min^{-1}. White light from the microscope source (WLS) was linearly polarized (P) before impinging on the sample inside the thermal chamber. After interacting with the sample, the transmitted light passed through the objective (HC PL FLUOTAR 10×/0.30 POL) and then through the analyzer (A), which was oriented orthogonally with respect to the polarizer P. The resulting image was captured by a complementary metal–oxide–semiconductor (CMOS) camera (Thorlabs CS126CU) and stored on a computer. Optionally, a quarter-wave plate (QWP) was inserted between the objective and the analyzer to generate circularly polarized light, thereby enabling visualization of the liquid crystal–air interface.

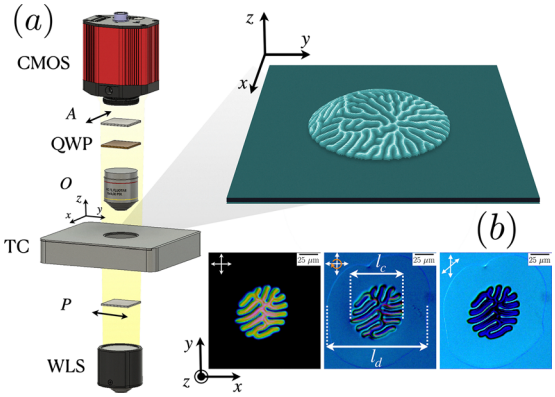

Fig. 1 Experimental observations of labyrinthine patterns in chiral liquid crystal droplets. (a) Schematic representation of the light path in the polarized optical microscopy setup. White light from the source (WLS) is linearly polarized by the polarizer (P). The polarized light interacts with a droplet of chiral liquid crystal on a glass slide inside a thermal chamber (TC). The transmitted light is collected by the objective (O). Then it passes through the analyzer (A) crossed with respect to P, and is captured by the metal–oxide–semiconductor (CMOS) camera. The light can pass through a quarter-wave plate (QWP). The inset shows a schematic representation of the liquid crystal droplet. (b) Comparison of optical textures under different polarization conditions for a droplet with 10 wt% chiral dopant concentration at 50 °C. The polarization configuration for each panel is indicated by the symbols in the upper-left corners: crossed white arrows denote observation between crossed polarizers (left panel), the orange circular arrow signifies the insertion of a QWP (central panel), and white arrows at 45° indicate polarizers oriented at a 45-degree angle to each other (right panel). The labels l_c and l_d represent the characteristic lengths of the confined labyrinthine pattern and the total droplet, respectively. The difference between these values illustrates the wetting region at the droplet's periphery, where the thickness $d(r)$ is too small to support the winding/unwinding transition, keeping the liquid crystal in an unwound homeotropic state.

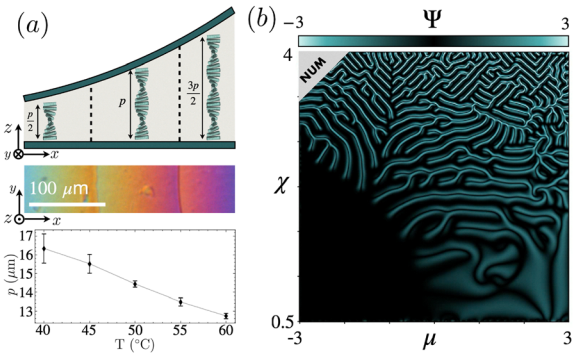

Fig. 2 Chiral pitch characterization as a function of temperature and texture mapping of model eqn (2) in the parameter space. (a) Experimental measurement of the cholesteric pitch p using the Grandjean-Cano technique. The top panels show a schematic of the experimental setup and a representative polarized optical microscopy snapshot of the disclination lines. The bottom panel displays the temperature dependence of the pitch $p(T)$ for the E7 mixture doped with 10 wt% EOS-12; error bars correspond to the standard error of the measurements. (b) Polarized field Ψ = Re(A)Im(A) obtained by numerical simulation of model eqn (2) in an inhomogeneous parameter space. The horizontal and vertical axes represent lineal variations in the bifurcation parameter μ and the chirality parameter χ, respectively, mapping the transition between different self-organized textures supported by amplitude eqn (2). Simulation parameters: β = 1 and δ = 0.05.

To establish a direct link between the material properties and the model parameters, the bulk cholesteric pitch p of the mixture was characterized as a function of temperature using the Grandjean-Cano technique (see Fig. 2a). This method uses a planoconvex lens with a radius of curvature R = 10.3 mm (Thorlabs) to modulate the liquid crystal thickness, producing characteristic disclination lines at thicknesses that are multiples of half the rotation length of the chiral liquid crystal.

Experimental results

At sufficiently high temperatures (over 30 °C), a confined labyrinthine pattern emerges within the droplets. Fig. 1b illustrates a confined labyrinthine pattern in a droplet with crossed polarizers and the same image using an additional quarter-wave plate. Observations were made over temperature ranges from 19 °C to 57 °C where the chiral phase is developed. In this

temperature range, at low temperatures, the liquid crystal presents in a winding configuration, with its molecules oriented vertically on average. We have called this configuration the homeotropic mesophase. As the temperature increases, the liquid crystal can transition to an unwinding state, in which the director, the average orientation of the molecules, begins to rotate about the vertical axis, which corresponds to a chiral phase. This transition is commonly known as winding/unwinding instability,[20] a result of the elastic effects that depend on anchoring conditions and thermal influences, determining the characteristic rotation length of molecular orientation. The rotation length is called pitch. The chiral phase is observed when the pitch approaches the droplet thickness.[20] As shown in the bottom panel of Fig. 2a, the pitch p of the E7 mixture with 10 wt% EOS-12 exhibits a monotonic decrease as temperature increases, allowing the chiral phase to extend into regions of smaller droplet thickness. To study the dynamics of the phase transition in CLC droplets and the emergence of disordered patterns, heating and cooling cycles were performed over these temperature ranges with a controlled ramp from 0.01 °C min^{-1} to 5 °C min^{-1}. It is important to note that temperature variations can affect both the optical ttures.[22] At room temperature (18 °C), the chiral liquid crystal sample exists in its homeotropic mesophase. As we gradually heat the sample, the chiral liquid crystal droplet undergoes a sudden transition at 32.2 °C, marked by the emergence of a chiral finger texture in the center of the droplet. As the temperature continues to rise, this texture begins to expand and eventually fills the entire droplet. Indeed, given the inhomogeneity of the droplet's thickness, the pattern tends to develop first in the center, where the thickness is most pronounced, and then expand as the temperature-induced change in pitch occurs. This localization is consistent with the variable-thickness profile resulting from the wetting and spreading of the liquid crystal on the glass slide. As shown in Fig. 1b, while the droplet extends to a total size l_d, the labyrinthine pattern remains restricted to a central region with a characteristic length l_c. In the outer region, the strong confinement prevents the development of the helical phase, leaving the material in an unwound state even when the center is fully patterned. Even as the temperature increases further, remaining above the winding/unwinding transition point to the chiral phase, the texture of the chiral droplet does not undergo significant changes. As the temperature gradually decreases, the chiral texture within the chiral liquid crystal droplet remains stable until it reaches 22.3 °C, at which point it abruptly disappears, leading to the formation of a homeotropic mesophase. Hence, under crossed polarizers, the droplets become completely black. This observation indicates that the winding/unwinding transition is subcritical in nature, exhibiting a hysteresis of approximately 10 °C. Fig. 3 illustrates these two mesophases and their respective subcritical transition.

Fig. 4 presents a series of snapshots that illustrate the development of the labyrinthine pattern. From these images,

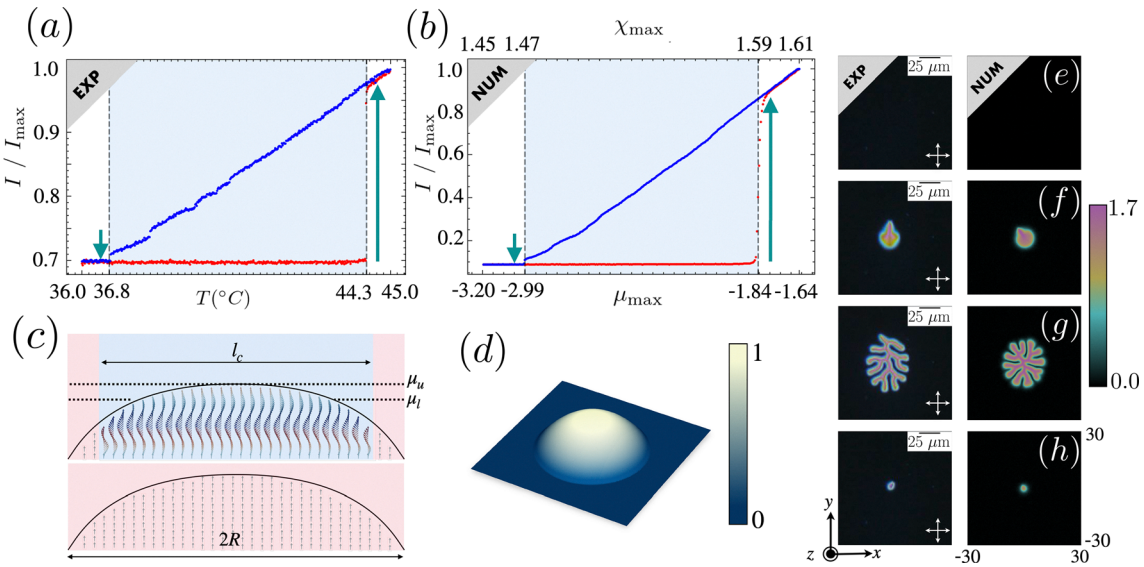

Fig. 3 Bistability in chiral liquid crystal droplets. (a) Normalized intensity I/I_{max}, where I_{max} is the maximum intensity, as a function of temperature from experimental measurements of a droplet with 10 wt% chiral dopant concentration. (b) Normalized intensity $\int\int|\mathcal{A}|^2 ds$ as a function of the maximum value $\mu_{max} = \max(\mu(r))$ control parameter from numerical simulations of the amplitude eqn (2). Simulation parameters: $\beta = 1$, $\delta = 0.05$, $\mu_0 = -6.7$, $\chi_0 = 1.1$, $\mu_1 = 2130$, $\chi_1 = 213$, $R = 22$, $a = 1$ and $b = 1.2$. The spatial dependence of the parameters is given by $\mu(r) = \mu_0 + \mu_1 (1 - (r/R)^2)/R^2$ and $\chi(r) = \chi_0 + \chi_1 (1 - (r/R)^2)/R^2$, with $r = ((x/a)^2 + (y/b)^2)^{1/2}$. In both upper panels, red dots denote the forward ramp (increasing μ and χ in simulation, heating in experiment), blue circles denote the reverse ramp (decreasing parameter or cooling), and the light blue shaded region indicates the bistability region. (c) Cross-sectional scheme of a droplet indicating characteristic lengths (l_c, R). The upper and lower images display the chiral and homeotropic mesophases, respectively. (d) 3D representation of the normalized droplet profile $d(r)$. (e)–(h) Representative textures from experiment (left panels) and simulations (right panels, showing the magnitude $|A|$) for different stages of the bistable transition. (e) Homeotropic mesophase. (f) Emergence of the first cholesteric finger upon heating (or increasing time in simulations). (g) More developed and branched cholesteric fingers. (h) Final stage upon cooling (or decreasing time in simulations), where a residual isolated point-like structure remains visible. The complete temporal dynamics of this bistable transition can be visualized in the SI (see Video[31]).

we can see how the cholesteric fingers create a confined labyrinthine structure. It is important to note that the cholesteric fingers typically align either perpendicular or parallel to the edges.

Theoretical description

Nematic and chiral liquid crystals are characterized by the fact that the molecules locally have an orientation order but not a positional one.[20,25]

Thus, to account for these soft materials at fixed temperature, one introduces the director $\boldsymbol{n}(\vec{r},t)$, which represents the average molecular orientation, where $\vec{r}$ and t represent the spatial coordinate and time.

For a chiral liquid crystal droplet with homeotropic anchoring close to winding/unwinding transition, the director is described by

$$\boldsymbol{n} = \begin{pmatrix} \cos\left(\frac{z}{p}+\theta\right)\sin\left[\alpha\sin\left(\frac{\pi z}{d}\right)\right] \\ \sin\left(\frac{z}{p}+\theta\right)\sin\left[\alpha\sin\left(\frac{\pi z}{d}\right)\right] \\ \cos\left[\alpha\sin\left(\frac{\pi z}{d}\right)\right] \end{pmatrix} \quad (1)$$

where $\alpha(x, y, t)$ and $\theta(x, y, t)$ are the polar and azimuthal angles the director forms concerning the vertical direction of the droplet. z represents the vertical coordinate. Let us consider flattened droplets, in which $d(r) = (1 - (r/R)^2)(2V/\pi R^2)$ denotes the thickness of the liquid crystal droplet, where r is a radial coordinate with origin in the droplet center, and V and R are the volume and horizontal radius of the droplet.[26] Fig. 3d illustrates the shape of the liquid crystal droplet by graphing $d(r)$. The dynamics of the director are characterized by the minimization of the Frank–Oseen free energy.[20,25] Thermal effects can be incorporated through the elastic constants, particularly by considering the variation in the pitch, which accounts for chirality χ.[21] For the liquid crystal we are studying, chirality is a monotonic function of temperature.[27] The physics of liquid crystals confined in cells that impose controlled anchoring is simpler than the physics of droplets, which also involves complex effects such as surface tension, gravity, surface energy, and roughness. All these effects determine the shape and curvature of the droplet. To shed light on the observed confined patterns, we will model the droplet near the winding/unwinding transition, where the curvature is assumed to be large (flattened shapes).

Close to the winding/unwinding transition, the marginal state is the homeotropic one, $\boldsymbol{n} = (0, 0, 1)$. Taking into account that the director is slightly deformed from the z-axis ($\alpha \ll 1$), giving rise to a chiral structure, the order parameter that characterizes this transition is $Ae^{iz/p}\sin(\pi z/d)$,[28] where the two-dimensional complex amplitude is defined as $A(x, y, t) \equiv \alpha(x, y, t)e^{i\theta(x,y,t)}$, which accounts for the projection of the director into the xy-plane. Employing the equation of the director close to the winding/unwinding transition, using expression (1) for small α, and through weakly nonlinear analysis, the amplitude A satisfies the equation (dimensionless chiral-anisotropic Ginzburg–Landau amplitude equation)[21,29]

$$\partial_t A = \mu(r)A + \beta A|A|^2 - A|A|^4 + \partial_{\eta\bar{\eta}}A + \delta\partial_{\eta\eta}\bar{A} + \chi(r)(A\partial_{\bar{\eta}}A - \bar{A}\partial_{\eta}A) \quad (2)$$

where $\mu(r) \equiv 2(2C(r) - K_{32})$ is the bifurcation parameter that characterizes the winding/unwinding transition, accounting for both geometric confinement and elastic effects. In particular, it reflects the competition between elastic distortions that favor a uniform alignment of the director field and those that promote its rotation. Here, $C(r) = d(r)/p$ is the confinement parameter, $K_{32} \equiv K_3/K_2$ and $K_{12} \equiv K_1/K_2$ are dimensionless parameters, $\{K_1, K_2, K_3\}$ are the splay, twist, and bend elastic constants.[20,25]

Although our mixture includes 10 wt% of the EOS-12 dopant, the elastic properties of the medium are fundamentally determined by the nematic host, E7. The temperature dependence of these constants for pure E7 has been characterized in ref. 30, showing that while the absolute values of the elastic constants decrease monotonically as temperature increases, the ratio K_{21} remains remarkably constant over a wide thermal range, while K_{31} exhibits a more pronounced decrease near the nematic–isotropic transition. The coefficient $\beta \equiv -(3 + K_{12} - 6K_{32} + 6C(r))(2/5Q)^{1/2}$ with $Q = K_{32} - 0.53K_{12} - 2.1/K_{32} + 0.22K_{12}/K_{32} + 1.18$ determines the nature of the bifurcation; in our experimental mixture, $\beta > 0$, indicating a subcritical transition. Namely, the system represents a winding/unwinding transition with a hysteresis loop. $\delta \equiv (K_{12} - 1)/2(K_{12} + 1)$ accounts for anisotropic coupling, arising from the competition between the elastic constants. The parameter $\chi(r) = [3 - 4K_{32} + K_{12} + 3C(r)]\Big/\left(2\sqrt{2}\sqrt{1 + K_{12}}\right)(8/5Q)^{1/4}$ is the chiral parameter, responsible for the breaking of mirror symmetry, thereby favoring chiral spatial modulations. This parameter is modulated by the confinement parameter and thus controlled by temperature changes. $\partial_\eta = \partial_x + i\partial_y$ is a differential operator on the

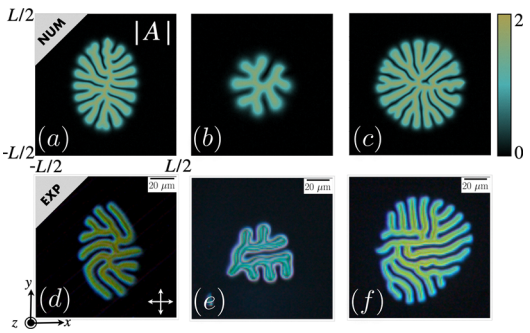

Fig. 4 Time evolution of a simulated chiral liquid crystal droplet obtained from numerical simulation of model eqn (2) compared with experiment. The experimental droplet is composed of EOS-12 at 10 wt%. Rows correspond to different time steps (t_1, t_2, t_3). Columns represent different calculated fields: the magnitude of the amplitude field A, the polarization field Ψ = Re(A)Im(A), and the phase field ϕ = arctan[Im(A)/Re(A)]. The rightmost column shows the corresponding experimental POM image for direct comparison. Simulation parameters: $\mu_0 = -5.5$, $\chi_0 = 1.2$, $\mu_1 = 3340$, $\chi_1 = 375$, $R = 25$ and $a = b = 1$.

complex plane, the Wirtinger derivative. $\bar{A}$ accounts for the complex conjugate of A. A detailed derivation of the amplitude eqn (2) from first principles is presented in ref. 21.

Note that $\mu(r)$ and $\chi(r)$ act as the primary control parameters of the system, as both depend on the confinement ratio $C = d(r)/p$. Since the pitch p decreases with temperature in our experimental mixture, and the thickness $d(r)$ varies across the droplet, changes in temperature directly modify C and, consequently, the local values of $\mu(r)$ and $\chi(r)$. In this way, these parameters effectively couple temperature and geometry to the system dynamics. To illustrate the robustness of this theoretical framework, Fig. 2b shows a numerical texture map of the polarized field Ψ in the (μ,χ) parameter space, identifying the transition regions between homeotropic states and labyrinthine textures.

Although the nonlinear coefficient β also depends on C, its role is to determine the nature of the bifurcation and the amplitude of the solution, rather than to control the onset or qualitative structure of the patterns. The dependencies of the coefficients of the remaining elastic constants primarily affect quantitative characteristics, such as branch width, without altering the underlying self-organization mechanism.

The amplitude eqn (2) shows a subcritical transition between the homeotropic mesophase ($A = 0$) and the chiral phase. Fig. 3 summarizes the type of transition observed numerically as the bifurcation parameter increases (see video in the SI[31]). Fig. 4 illustrates the emergence of the confined labyrinth based on model eqn (2) and shows a comparison with experimental observations, highlighting a fair agreement between them. To better understand the labyrinthine pattern structure, we have studied the phase structure of the amplitude A, observing a similar structure to that of the magnitude of A. We have also studied the polarization field, which is identical to what is observed with crossed polarizers for nematic liquid crystals; we observe similar textures (see Fig. 4).

The shape of a droplet on a substrate in air is determined by the balance between surface tension, liquid–solid adhesion energies, interfacial tension, gravity, and substrate properties. Due to the interaction of the liquid crystals with the substrate, we observed droplets with diverse morphologies. Fig. 5 illustrates different droplets with different morphologies that exhibit labyrinthine patterns. We also performed numerical simulations of the model eqn (2) with various geometries and observed similar labyrinthine patterns.

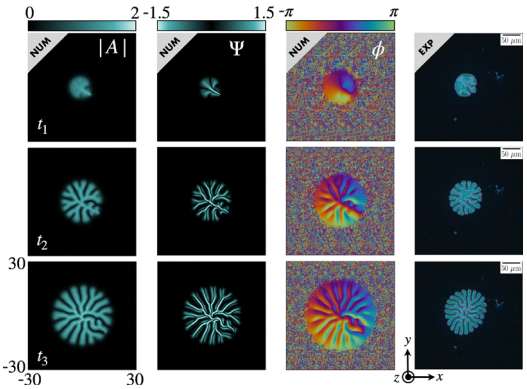

Fig. 5 Simulated and experimental patterns in chiral liquid crystal droplets with different shapes. The upper and lower panels correspond to numerical simulations and experimental observations, respectively. (a) Droplet with elongated shape given by the parameters $\mu_0 = -5.5$, $\chi_0 = 1.2$, $\mu_1 = 3340$, $\chi_1 = 375$, $R = 25$, $a = 1$ and $b = 1.5$. (b) Small droplet with parameters $\mu_0 = -5.5$, $\chi_0 = 1.2$, $\mu_1 = 1238$, $\chi_1 = 135$, $R = 15$ and $a = b = 1$. (c) Larger droplet with a weakly elongated shape given by the parameters $\mu_0 = -5.5$, $\chi_0 = 1.2$, $\mu_1 = 2764$, $\chi_1 = 276$, $R = 24$, $a = 1$ and $b = 1.1$. (d)–(f) Experimental counterparts to (a)–(c), respectively, observed at 50 °C, 22 °C and 55 °C. The chiral dopant concentration for the experimental samples (d)–(f) is 10 wt%.

Conclusions

In conclusion, our findings demonstrate that confined labyrinthine patterns in thermally induced chiral liquid crystal droplets arise from a discontinuous winding/unwinding transition. As the temperature increases, chiral fingers appear and invade the droplet center, generating stable confined labyrinthine patterns whose orientation depends on the boundary geometry. Using an adequate Ginzburg–Landau theoretical model, valid close to the winding/unwinding transition, we can describe the average orientational dynamics of the molecules, incorporating the effect of droplet size. Numerical simulations based on this model demonstrate qualitative agreement with the experimental results, validating the proposed theoretical approach and highlighting the role of confinement in the self-organization of chiral structures. Note that the observed phenomena are highly reproducible in their qualitative characteristics. While the specific morphology of each droplet is unique due to the roughness and inhomogeneities of the substrate and the capillary effect, the fundamental self-organization mechanism, specifically the emergence of the labyrinthine pattern and the subcritical nature of the transition, is consistent across all experiments. Our results highlight the fundamental role of confinement and geometry in the self-organization of chiral media and establish a minimal theoretical framework for describing confined pattern formation in soft matter systems.

The amplitude eqn (2) is a highly simplified theoretical model compared to the usual descriptions based on three-dimensional elasticity of the director. Together with the expression for the director, eqn (1), we can reconstruct the three-dimensional structure of molecular orientation, which is not accessible with simple experiments. Furthermore, this model allows us to understand other phenomena, such as the emergence and organization of spherolites and the transition between different textures. Beyond providing insight into the physics of chiral droplets, this study opens pathways for controlling defect-mediated textures in microstructured optical and responsive materials. Indeed, topological defects and different textures are relevant elements in the generation of light beams with topological properties.[34]

Systems that exhibit the coexistence of disordered patterns and homogeneous states can present a family of localized

labyrinthine patterns.[32,33] However, in our chiral liquid crystal droplets, we did not observe this phenomenon, presumably due to the slow variation in drop thickness.

Author contributions

M. R.-S. and M. G. C. wrote the original draft of the manuscript. M. R.-S. performed the research, analyzed the data, conducted numerical simulations and experimental observations, and designed the figures. All authors (M. R.-S., V. F.-G., M. G. C., P. I. H. and J. V.) participated in the discussion of the research and contributed to the revision and improvement of the final manuscript.

Conflicts of interest

There are no conflicts to declare.

Data availability

The data supporting the results reported in this article are available as follows: the numerical code used for the simulations of the chiral anisotropic Ginzburg–Landau amplitude equation has been deposited in Zenodo and can be accessed at https://doi.org/10.5281/zenodo.18507361, while a video illustrating the complete temporal dynamics of the experimental and numerical winding/unwinding transition is provided as part of the supplementary information (SI). Supplementary information is available. See DOI: https://doi.org/10.1039/d6sm00114a.

Acknowledgements

M. R.-S., V. F.-G., and M. G. C. acknowledge the financial support of ANID-Millennium Science Initiative Program-ICN17_012 (MIRO).

Notes and references

1 G. Nicolis and I. Prigogine, *Self-Organization in NonEquilibrium Systems*, Wiley, New York, 1977.
2 M. Cross and H. Greenside, *Pattern Formation and Dynamics in Non-Equilibrium Systems*, Cambridge University Press, New York, 2009.
3 L. Pismen, *Patterns and Interfaces in Dissipative Dynamics*, Springer, Berlin, 2006.
4 M. I. Rabinovich, A. B. Ezersky and P. D. Weidman, *The Dynamics of Patterns*, World Scientific, Singapore, 2000.
5 D. Walgraef, *Spatio-Temporal Pattern Formation: With Examples from Physics, Chemistry, and Materials Science*, Springer Science & Business Media, Berlin, 2012.
6 H. Reinken, *Controlling Mesoscale Turbulence: The Impact of Translational and Rotational Constraints on Pattern Formation in Microswimmer Suspensions*, Springer Theses, 2024.
7 R. B. Hoyle, *Pattern formation: an introduction to methods*, Cambridge University Press, Cambridge, 2006.
8 A. O. Leon, M. G. Clerc and S. Coulibaly, Dissipative structures induced by spin-transfer torques in nanopillars, *Phys. Rev. E:Stat., Nonlinear, Soft Matter Phys.*, 2014, **89**, 022908.
9 S. Echeverría-Alar and M. G. Clerc, Labyrinthine patterns transitions, *Phys. Rev. Res.*, 2020, **2**, 042036.
10 Q. X. Liu, P. M. Herman, W. M. Mooij, J. Huisman, M. Scheffer, H. Olff and J. Van De Koppel, Pattern formation at multiple spatial scales drives the resilience of mussel bed ecosystems, *Nat. Commun.*, 2014, **5**, 5234.
11 A. Yochelis, Y. Tintut, L. L. Demer and A. Garfinkel, The formation of labyrinths, spots and stripe patterns in a biochemical approach to cardiovascular calcification, *New J. Phys.*, 2008, **10**, 055022.
12 J. von Hardenberg, E. Meron, M. Shachak and Y. Zarmi, Diversity of Vegetation Patterns and Desertification, *Phys. Rev. Lett.*, 2001, **87**, 198101.
13 I. R. Epstein and V. K. Vanag, Complex patterns in reactive microemulsions: Self-organized nanostructures?, *Chaos*, 2005, **15**, 047510.
14 R. Barrio, C. Varea, J. Aragón and P. Maini, A two-dimensional numerical study of spatial pattern formation in interacting Turing systems, *Bull. Math. Biol.*, 1999, **61**, 483.
15 S. W. Morris, E. Bodenschatz, D. S. Cannell and G. Ahlers, Spiral Defect Chaos in Large Aspect Ratio Rayleigh-Bénard *Convection*, *Phys. Rev. Lett.*, 1993, **71**, 2026.
16 Z. Khattari and T. M. Fischer, Shapes of Langmuir monolayer domains in confined geometries, *J. Phys. Chem. B*, 2002, **106**, 1677.
17 R. E. Rosensweig, M. Zahn and R. Shumovich, Labyrinthine instability in magnetic and dielectric fluids, *J. Magn. Magn. Mater.*, 1983, **39**, 127.
18 K. J. Lee, W. McCormick, Q. Ouyang and H. L. Swinney, Pattern formation by interacting chemical fronts, *Science*, 1993, **261**, 192.
19 P. Oswald, J. Baudry and S. Pirkl, Static and dynamic properties of cholesteric fingers in electric field, *Phys. Rep.*, 2000, **337**, 67.
20 P. Oswald and P. Pieranski, *Nematic and Cholesteric Liquid Crystals*, CRC Press, 2005.
21 S. Echeverría-Alar, M. G. Clerc and I. Bordeu, Emergence of disordered branching patterns in confined chiral nematic liquid crystals, *Proc. Natl. Acad. Sci. U. S. A.*, 2023, **120**, e2221000120.
22 V. Fernandez-Gonzalez, S. Echeverría-Alar, J. Vergara, P. I. Hidalgo and M. G. Clerc, Topological transition between disordered patterns through heating rate-induced defect emergence, *Chaos, Solitons Fractals*, 2024, **180**, 114508.
23 V. Fernandez-Gonzalez, M. G. Clerc, G. González-Cortés, P. I. Hidalgo and J. Vergara, Abrikosov clusters in chiral liquid crystal droplets, *Rep. Prog. Phys.*, 2024, **87**, 120502.
24 M. L. Parra, P. I. Hidalgo and E. Y. Elgueta, Synthesis and mesomorphic properties of oxadiazole esters derived from (R)-2-octanol,(S)-2-n-octyloxypropanol and (2 S, 3 S)-2-chloro-3-methylpentanol, *Liq. Cryst.*, 2008, **35**, 823.

25 P. de Gennes and J. Prost, *The Physics of Liquid Crystals, International series of monographs on physics*, Clarendon Press, 1993.
26 D. Bonn, J. Eggers, J. Indekeu, J. Meunier and E. Rolley, Wetting and spreading, *Rev. Mod. Phys.*, 2009, **81**, 739.
27 M. G. Clerc, A. H. Cornejo, S. Echeverría-Alar, G. González-Cortés, P. I. Hidalgo, P. J. Luo, M. J. Morel, J. Vergara and M. Wilson, Chirality transfer to harness mesophase transitions in liquid crystal mixtures containing an oxadiazole derivative, *Liq. Cryst.*, 2023, **50**, 1938.
28 T. Frisch, L. Gil and J. M. Gilli, Two-dimensional Landau-De Gennes dynamical model for the unwinding transition of a cholesteric liquid crystal, *Phys. Rev. E:Stat. Phys., Plasmas, Fluids, Relat. Interdiscip. Top.*, 1993, **48**, R4199.
29 M. G. Clerc, G. González-Cortés and S. Echeverría-Alar, Localized dissipative vortices in chiral nematic liquid crystal cells, *Phys. Rev. Res.*, 2022, **4**, L022021.
30 H. Hakemi, E. F. Jagodzinski and D. B. Dupré, Temperature dependence of the anisotropy of turbidity and elastic constants of nematic liquid crystal mixture E7, *Mol. Cryst. Liq. Cryst.*, 1983, **91**, 129.
31 See SI for a video, which illustrates how the droplet's textures are modified as a function of the bifurcation parameter, both through experimental observation and numerical simulation.
32 M. G. Clerc, S. Echeverria-Alar and M. Tlidi, Localised labyrinthine patterns in ecosystems, *Sci. Rep.*, 2021, **11**, 18331.
33 M. G. Clerc, S. Echeverria-Alar and M. Tlidi, Localized states with nontrivial symmetries: Localized labyrinthine patterns, *Phys. Rev. E*, 2022, **105**, L012202.
34 R. Barboza, U. Bortolozzo, G. Assanto, E. Vidal-Henriquez, M. G. Clerc and S. Residori, Vortex Induction *via* Anisotropy Stabilized Light-Matter Interaction, *Phys. Rev. Lett.*, 2012, **109**, 143901.